Internal electron transport barrier due to neoclassical ambipolarity in the Helically Symmetric Experimenta)

J. Lore, W. Guttenfelder, A. Briesemeister, D. T. Anderson, F. S. B. Anderson, C. B. Deng, K. M. Likin, D. A. Spong, J. N. Talmadge, and K. Zhai

Citation: Physics of Plasmas **17**, 056101 (2010); doi: 10.1063/1.3300465
View online: http://dx.doi.org/10.1063/1.3300465
View Table of Contents: http://scitation.aip.org/content/aip/journal/pop/17/5?ver=pdfcov
Published by the AIP Publishing

Internal electron transport barrier due to neoclassical ambipolarity in the Helically Symmetric Experiment[a)]

J. Lore,[1,b)] W. Guttenfelder,[2] A. Briesemeister,[1] D. T. Anderson,[1] F. S. B. Anderson,[1] C. B. Deng,[3] K. M. Likin,[1] D. A. Spong,[4] J. N. Talmadge,[1] and K. Zhai[1]
[1]*Department of Electrical and Computer Engineering, University of Wisconsin - Madison, Madison, Wisconsin 53706, USA*
[2]*Department of Physics, University of Warwick, Coventry CV4 7AL, United Kingdom*
[3]*Department of Physics, University of California - Los Angeles, Los Angeles, California 90024, USA*
[4]*Oak Ridge National Laboratory, Oak Ridge, Tennessee 37831, USA*

(Received 20 November 2009; accepted 6 January 2010; published online 4 February 2010)

Electron cyclotron heated plasmas in the Helically Symmetric Experiment (HSX) feature strongly peaked electron temperature profiles; central temperatures are 2.5 keV with 100 kW injected power. These measurements, coupled with neoclassical predictions of large "electron root" radial electric fields with strong radial shear, are evidence of a neoclassically driven thermal transport barrier. Neoclassical transport quantities are calculated using the PENTA code [D. A. Spong, Phys. Plasmas **12**, 056114 (2005)], in which momentum is conserved and parallel flow is included. Unlike a conventional stellarator, which exhibits strong flow damping in all directions on a flux surface, quasisymmetric stellarators are free to rotate in the direction of symmetry, and the effect of momentum conservation in neoclassical calculations may therefore be significant. Momentum conservation is shown to modify the neoclassical ion flux and ambipolar ion root radial electric fields in the quasisymmetric configuration. The effect is much smaller in a HSX configuration where the symmetry is spoiled. In addition to neoclassical transport, a model of trapped electron mode turbulence is used to calculate the turbulent-driven electron thermal diffusivity. Turbulent transport quenching due to the neoclassically predicted radial electric field profile is needed in predictive transport simulations to reproduce the peaking of the measured electron temperature profile [Guttenfelder *et al.*, Phys. Rev. Lett. **101**, 215002 (2008)]. © *2010 American Institute of Physics*. [doi:10.1063/1.3300465]

I. INTRODUCTION

The Helically Symmetric Experiment[1] (HSX) is a four field period quasisymmetric stellarator, designed to have a magnetic field strength $|B|$ dominated by a single $(n,m)=(4,1)$ helical Fourier spectral component, where $|B|$ on a surface labeled by ρ is written $B(\rho,\theta,\phi)=B_0\Sigma_{m,n}b_{m,n}(\rho\cos(n\phi-m\theta))$. In the quasihelically symmetric (QHS) configuration of HSX the symmetry spoiling spectral components are smaller than 1% at the plasma edge. Quasisymmetric configurations have been shown to have zero net radial drifts of particles from a flux surface[2,3] and small flow damping in the symmetry direction[4,5] allowing for free rotation.[6] HSX has experimentally demonstrated reduced particle, heat,[7] and momentum transport[4] and improved confinement of energetic particles[8,9] as compared to a conventional stellarator, with reductions consistent with neoclassical theory.

With the reduction in neoclassical transport in HSX, the anomalous contribution to the total transport is dominant across the plasma radius. For this reason, methods of reducing the turbulent transport are of particular interest. The impact of the HSX geometry on anomalous transport has been investigated using transport modeling[10] and probe measurements.[11] As will be discussed below, the internal transport barrier in QHS is observed in the same region as significant $\mathbf{E}\times\mathbf{B}$ flow shear predictions. The flow profile results in shearing rates that are much larger than the maximum linear growth rate in the plasma core, therefore turbulence "quenching" is expected. The reduction in both turbulent and neoclassical transport can result in high temperatures and peaked temperature profiles even for a relatively small amount of input power.

A combination of centrally peaked electron temperature profiles and large, positive "electron root" radial electric fields (E_r) has been observed in several stellarators.[12–15] This class of internal transport barriers has been collectively named core electron root confinement (CERC).[16,17] Large radial electric fields are important, particularly in conventional stellarators, as they act to pull both plasma species out of the detrimental "$1/\nu$" regime that can result in large neoclassical transport. The E_r profile may also have significant radial shear and act to reduce turbulent transport. Reduction in turbulent transport in CERC plasmas has been both measured[18] and modeled.[10,19] Because the radial electric field profile is determined from the *nonambipolar* neoclassical fluxes by enforcing ambipolarity on each flux surface, this type of transport barrier is unique to stellarators.

Another common feature of CERC transport barriers is the existence of thresholds for achieving a CERC in injected electron cyclotron resonance heating (ECRH) power P_{inj} and

[a)]Paper NI3 6, Bull. Am. Phys. Soc. **54**, 182 (2009).
[b)]Invited speaker. Electronic mail: jlore@wisc.edu.

electron density n_e.[16,17] Specifically, CERC behavior is only seen above a threshold value of P_{inj}/n_e. These experimental observations have been attributed to ECRH effects, such as "convective" fluxes driven by heating ripple trapped populations of electrons. Because the threshold P_{inj}/n_e has been observed to be lower in the configuration with larger on-axis ripple at the Wendelstein 7-AS stellarator (W7-AS)[20,21] and in the device with the largest effective ripple (TJ-II) in an intermachine comparison,[17] it had been suggested that the power threshold in a quasisymmetric device may be very high.[17] Here it will be shown that despite a small effective ripple, a CERC can exist in the QHS configuration of HSX for a sufficiently large ratio of T_e/T_i.

The plasmas discussed in this work are heated with $\leq$100 kW of ECRH, with an on-axis magnetic field strength of $B_0=1.0$ T. During ECRH, electron temperature (T_e) profiles are measured to be very centrally peaked, with core temperatures of 2.5 keV for 100 kW of injected power. The ion temperatures (T_i), on the other hand, are less than 100 eV across the plasma radius. These temperature profiles, in particular, the large ratio of T_e/T_i, result in large, positive electron root radial electric field predictions in the plasma core and small "ion root" predictions across most of the plasma radius.

Neoclassical transport calculations are performed using the PENTA code[5] in which momentum conservation is enforced using a moments method.[22] Momentum is conserved by including the effect of parallel flow, which is often neglected in stellarator neoclassical transport calculations[23] due to the strong flow damping exhibited in all directions on a flux surface in a conventional stellarator.[24,25] The assumption of negligible parallel flow is generally not justified in quasisymmetric configurations, where flow damping is reduced in the direction of symmetry, and parallel flow can be significant.[5]

Section II discusses the neoclassical transport calculations performed by PENTA. The neoclassically determined radial electric field profile and the mechanism that leads to large positive E_r in the core with a region of strong radial shear are described in Sec. III. In Sec. IV the coupled neoclassical and turbulent transport simulations are discussed, in particular, how the neoclassically determined radial electric field profile leads to quenching of the turbulent transport. The effect of strong E_r and momentum conservation on the neoclassical transport calculations is shown in Sec. V. Finally, conclusions are given in Sec. VI.

II. DESCRIPTION OF THE NEOCLASSICAL TRANSPORT CALCULATIONS

The neoclassical transport calculations discussed in this work were performed using the PENTA code, based on the momentum-conserving moments method of Sugama and Nishimura.[22] PENTA uses a database of transport coefficients calculated using the DKES code,[26,27] which solves the linearized drift kinetic equation (DKE) using a pitch angle scattering (PAS) collision operator. The simplified collision operator neglects field particle collisions, which decouples the DKE of each species. Further, the particle speed v is conserved, reducing the dimensionality of the problem. These simplifications allow for efficient and fast calculation of neoclassical transport coefficients for many radii, collision frequencies, and radial electric fields for an arbitrary number of $|B|$ spectral components. On the other hand, the PAS operator does not conserve momentum, does not allow for proper calculation of the parallel flows (and therefore bootstrap current), and the transport coefficients do not recover the intrinsic ambipolarity in ideal (quasi)symmetric systems.

Momentum conservation is enforced through the $l=2$ Legendre component of the guiding center distribution function f_1, from which the viscosity coefficients are derived. The field particle collisions can be neglected in the calculation of the viscosity coefficients because the $l=2$ component of f_1 is dominated by test particle collisions.[28] In this sense the momentum is conserved at a macroscopic level instead of a microscopic (kinetic) level. In Ref. 22 it is shown how to calculate the viscosity coefficients from the DKES output. In this method the $l=1$ component of f_1 and the momentum-conserving collision operator are expanded in a series of Sonine (associated Laguerre) polynomials. In this section only the first two polynomials are retained for notational brevity.

The particle and heat fluxes for a species a are calculated from a linear combination of thermodynamic forces and parallel flows as

$$\begin{bmatrix} \Gamma_a^{bn} \\ q_a^{bn}/T_a \end{bmatrix} = N_a \begin{bmatrix} U_{\|a} \\ Q_{\|a} \end{bmatrix} + L_a \begin{bmatrix} X_{a1} \\ X_{a2} \end{bmatrix}. \tag{1}$$

The "banana-nonaxisymmetric" particle and conductive heat fluxes are defined as the total flux minus the Pfirsch–Schlüter flux, $\Gamma_a^{bn} \equiv \langle \int d^3v g_a \mathbf{v}_{da} \cdot \nabla \rho \rangle - \Gamma_a^{PS}$ and $q_a^{bn} \equiv T_a \langle \int d^3v g_a \mathbf{v}_{da} \cdot \nabla \rho (x_a^2 - 5/2) \rangle - q_a^{PS}$,[29,30] respectively, where $\mathbf{v}_{da}$ is the guiding center drift velocity,[27,22] $x_a \equiv v/v_{Ta}$, and $g_a = f_{a1} - f_{a1}^{(l=1)}$ is the first order distribution function minus the first Legendre component. The thermodynamic forces are $X_{a1} \equiv -p_a'/n_a - e_a \Phi'$ and $X_{a2} \equiv -T_a'$, with the pressure $p_a \equiv n_a T_a$, and n_a and T_a, are the species' density and temperature, respectively. The ($'$) denotes a radial derivative, and the electric field is defined as $\mathbf{E} \equiv -\nabla \Phi$.

The parallel particle and heat flows, defined as $U_{\|a} \equiv \langle B u_{\|a} \rangle / \langle B^2 \rangle$ and $Q_{\|a} \equiv (2/5 p_a) \langle B q_{\|a} \rangle / \langle B^2 \rangle$, respectively, are calculated from the friction-flow relations and parallel momentum balance equations as

$$\begin{aligned} (M_a - \langle B^2 \rangle l_{aa}) \begin{bmatrix} U_{\|a} \\ Q_{\|a} \end{bmatrix} - \langle B^2 \rangle \sum_{b \neq a} l_{ab} \begin{bmatrix} U_{\|b} \\ Q_{\|b} \end{bmatrix} \\ = -N_a \begin{bmatrix} X_{a1} \\ X_{a2} \end{bmatrix} + \begin{bmatrix} n_a e_a \langle B^2 \rangle^{1/2} \\ 0 \end{bmatrix} \frac{\langle B E_{\|} \rangle}{\langle B^2 \rangle^{1/2}}. \end{aligned} \tag{2}$$

In Eqs. (1) and (2), the coefficients

$$N_a \equiv \begin{bmatrix} N_{a1} & N_{a2} \\ N_{a2} & N_{a3} \end{bmatrix}, \quad L_a \equiv \begin{bmatrix} L_{a1} & L_{a2} \\ L_{a2} & L_{a3} \end{bmatrix}, \quad M_a \equiv \begin{bmatrix} M_{a1} & M_{a2} \\ M_{a2} & M_{a3} \end{bmatrix} \tag{3}$$

are defined in Ref. 22, and the classical friction coefficients

$$l_{ab} \equiv \begin{bmatrix} l_{11}^{ab} & -l_{12}^{ab} \\ -l_{21}^{ab} & l_{22}^{ab} \end{bmatrix} \quad (4)$$

(for low orders) in Refs. 28 and 31. Equations (1) and (2) are given for an arbitrary order in the Sonine expansion in Ref. 29; for a nearly equivalent method, see Refs. 32 and 33. Reference 33 also describes a "direct" momentum correction method, which is a generalization of the classical Spitzer problem.[34]

The coefficients in Eq. (3) are calculated from a database of monoenergetic coefficients from the DKES code, although Monte Carlo methods are also being developed.[35] The method described above has been shown to analytically reproduce intrinsic ambipolarity in the (quasi)symmetric limit, which is currently being investigated numerically. The use of monoenergetic coefficients, while extremely attractive from the standpoint of computation, presents several difficulties in the presence of strong radial electric fields. These issues are discussed in Sec. V.

Setting the parallel flow to zero and dropping corrections to the L coefficient due to momentum conservation reduces Eq. (1) to give the "conventional" stellarator neoclassical fluxes calculated from direct energy convolution of the monoenergetic coefficients (see Refs. 26 and 27). A comparison of neoclassical quantities with and without momentum conservation for HSX experimental parameters is given in Sec. V.

III. RADIAL ELECTRIC FIELD PROFILE

The radial electric field is a critical transport quantity in stellarators as it can reduce both neoclassical transport through its magnitude and turbulent transport through its shear. The radial electric field in a nonsymmetric system is calculated by solving for the momentum relaxation on a flux surface.[36] The momentum relaxation can be described by the in-surface flows in two directions, such as the poloidal and toroidal flows. More commonly, the flow parallel to **B** ($U_\parallel$) and the radial electric field (which along with a diamagnetic component gives the perpendicular flow) are used.[36] In conventional stellarator neoclassical calculations the parallel flow is assumed to be negligible due to the strong flow damping. In this case solving for the momentum relaxation reduces to just enforcing ambipolarity of the nonambipolar particle fluxes to determine E_r,[37] with $U_\parallel$ neglected in Eq. (1), and Eq. (2) does not need to be solved. (The case of $U_\parallel \neq 0$ is accounted for in HSX neoclassical calculations, as described in Sec. II.) The so-called "ambipolarity constraint" can be written as

$$\sum_a e_a \Gamma_a = 0, \quad (5)$$

where the summation is over species, e_a is the species' charge, and Γ_a the particle flux. As Γ_a is a function of both E_r and the radial transport coefficients, Eq. (5) is a nonlinear equation that can have any odd number of solutions. A common scenario with $T_e \approx T_i$ and both species in the long mean free path (LMFP) regime results in three solutions, as shown in Fig. 1. The ion root typically occurs at a small, negative E_r

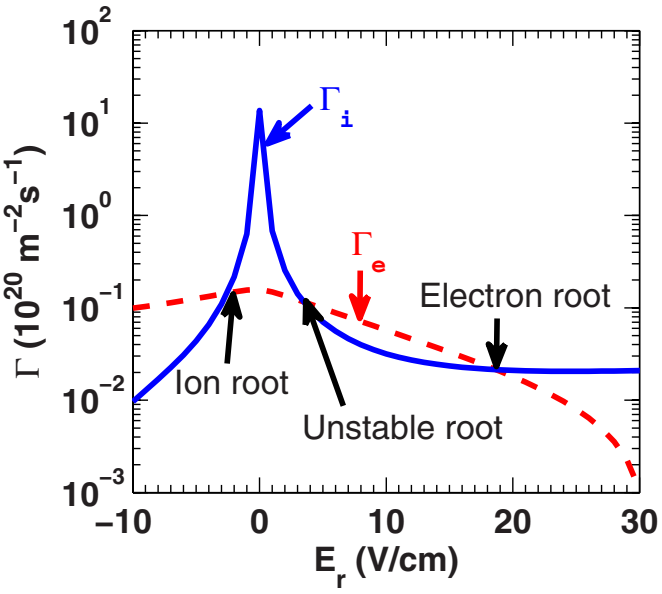

FIG. 1. (Color online) Neoclassical particle fluxes vs E_r for $T_e \approx T_i = 1$ keV. The three ambipolar roots are labeled, with the middle root unstable to perturbations in E_r.

where the primary effect is to reduce the ion flux from the $E_r=0$ level. The electron root occurs at a large, positive E_r where both species fluxes are strongly reduced from the $E_r=0$ level. In this sense the electron root represents an improved confinement regime. The intermediate root is thermodynamically unstable to perturbations in E_r, i.e., a perturbation in E_r results in a drive in the direction of the change.

In general, assuming an initial condition of zero radial electric field for the scenario described in Fig. 1, the plasma will be in the ion root in steady state as it cannot cross the unstable solution. In this case, one way to achieve the electron root is by increasing the electron flux, such that the plasma is driven over the unstable root, for example, from ECRH driven convective[21] or diffusive fluxes.[38] On the other hand, if $T_e \gg T_i$, the ion root may no longer exist near the plasma core. This is the situation that occurs in HSX plasmas, which have no direct ion heating. Typical measured electron temperature and density profiles from Thomson scattering are shown in Fig. 2. The electron temperature profile is strongly peaked inside of $r/a \approx 0.3$, and much larger than the ion temperature, Fig. 2(c), for $r/a \leq 0.5$.

The ion temperature profile, shown in Fig. 2(c), is measured by the ChERS system[39] from Doppler broadening of impurity emission of C+5 atoms. The measurement is from the "poloidal" ChERS view, and both fine structure broadening and the instrumental function have been taken into account. The precision of the measurement is limited by the signal strength, which is typically low near the plasma edge. Coronal equilibrium calculations using the atomic data and analysis structure[40] (ADAS) suggest that the neutral hydrogen density limits the ionization states present in the plasma. The energy transfer time between C+5 and protons has been calculated to be on the order of 0.02–0.04 ms, much shorter than the ion confinement time of 2–5 ms.[39,4]

At these ion temperatures (<100 eV) the ions experi-

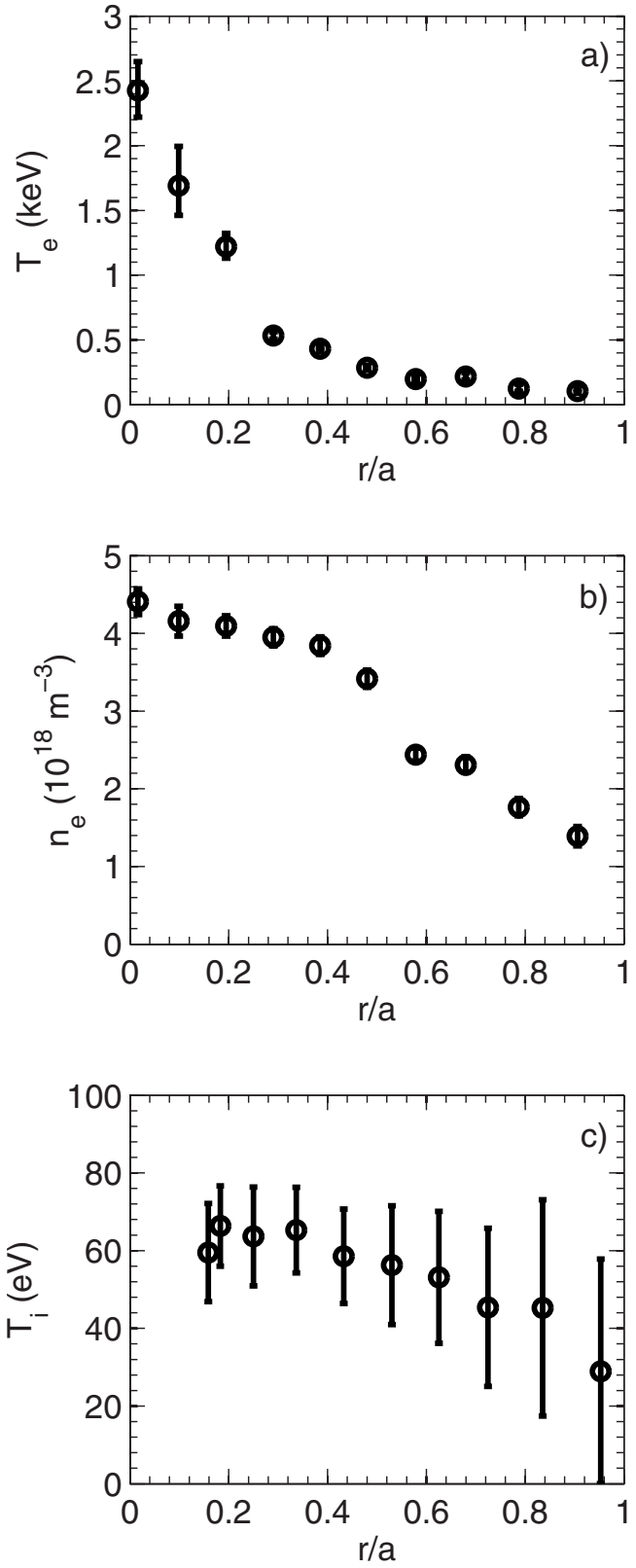

FIG. 2. (a) Measured electron temperature and (b) density profiles from Thomson scattering for a 100 kW QHS plasma. (c) Ion temperature profile measured by ChERS.

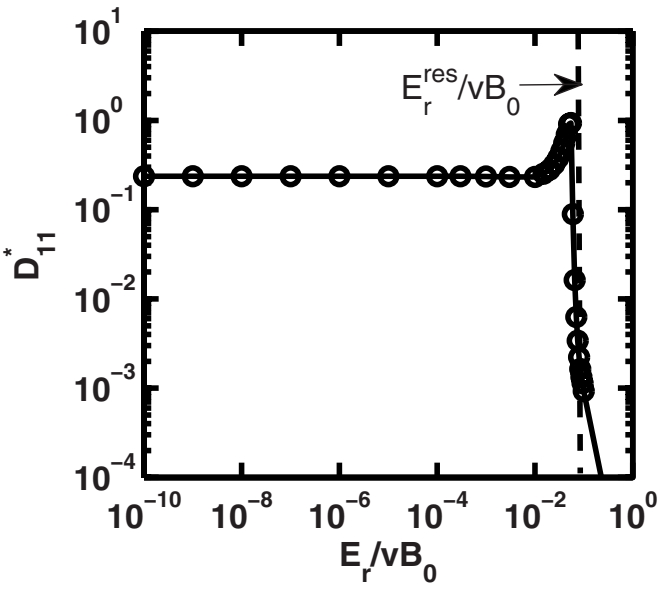

FIG. 3. Normalized monoenergetic transport coefficient $D_{11}^* \equiv D_{11}/(m_a^2 v^3/2e_a^2)$ vs E_r from DKES showing the peaking and reduction in transport due to the poloidal resonance.

ence a resonance at a relatively modest E_r near the plasma core.[41] The resonance occurs when the poloidal velocity of a passing particle as it follows a field line is cancelled by the poloidal component of the $\mathbf{E}\times\mathbf{B}$ drift, effectively resulting in a particle that sees zero rotational transform. For $E_r > E_r^{res} = (|m-nq|/m)v_{Ta}B_p$,[42] the fluxes are strongly reduced, corresponding to the situation in a symmetric system where the trapped particle fraction drops to zero.[41,43,33] This is captured in DKES calculations of the monoenergetic radial transport coefficient, as shown in Fig. 3 for $r/a \approx 0.2$. In QHS, only a single resonance corresponding to $(n,m)=(4,1)$ is seen; for a broader $|B|$ spectrum additional helical resonances can exist. Note that closer to the core additional resonances are found in QHS, as the symmetry breaking terms become larger relative to the (4,1) term.

The factor of $m-nq$ increases E_r^{res}/v by ~ 3 $(q \sim 1)$, as compared to an equivalent tokamak; however, for $T_i \leq 100$ eV this is still easily surpassed. The effect of the resonance on the ion particle flux can be clearly seen in Fig. 4. Neglecting the resonance, Γ_i scales linearly with E_r in this collisional regime. When the resonance is included, Γ_i has a maximum at E_r^{res} and decreases rapidly for larger E_r. The peaking in the flux is broader than that in the diffusion coefficient because of the energy convolution of the monoenergetic coefficients.

The E_r profile versus radius resulting from solving Eq. (5) is shown in Fig. 5. Three distinct regions can be seen, corresponding to the three scenarios described below. Near the plasma core [$r/a < 0.18$, Fig. 4(a)] the electron flux is much larger than the ion flux at $E_r=0$ and the ion flux is reduced to a small level due to the resonance. In this case a single ambipolar root occurs at a large positive E_r, essentially at $\Gamma_e \approx 0$; corresponding to the region of Fig. 5 of only electron root solutions. The region of $0.18 < r/a < 0.33$ [Fig. 4(b)] has three ambipolar roots (two stable): an ion root where the resonance pushes the ion flux through the electron flux and again an electron root near $\Gamma_e \approx 0$. Finally, across most of the plasma radius [$r/a > 0.33$, Fig. 4(c)] the electron flux is small (due to the reduced T_e), and only ion root solu-

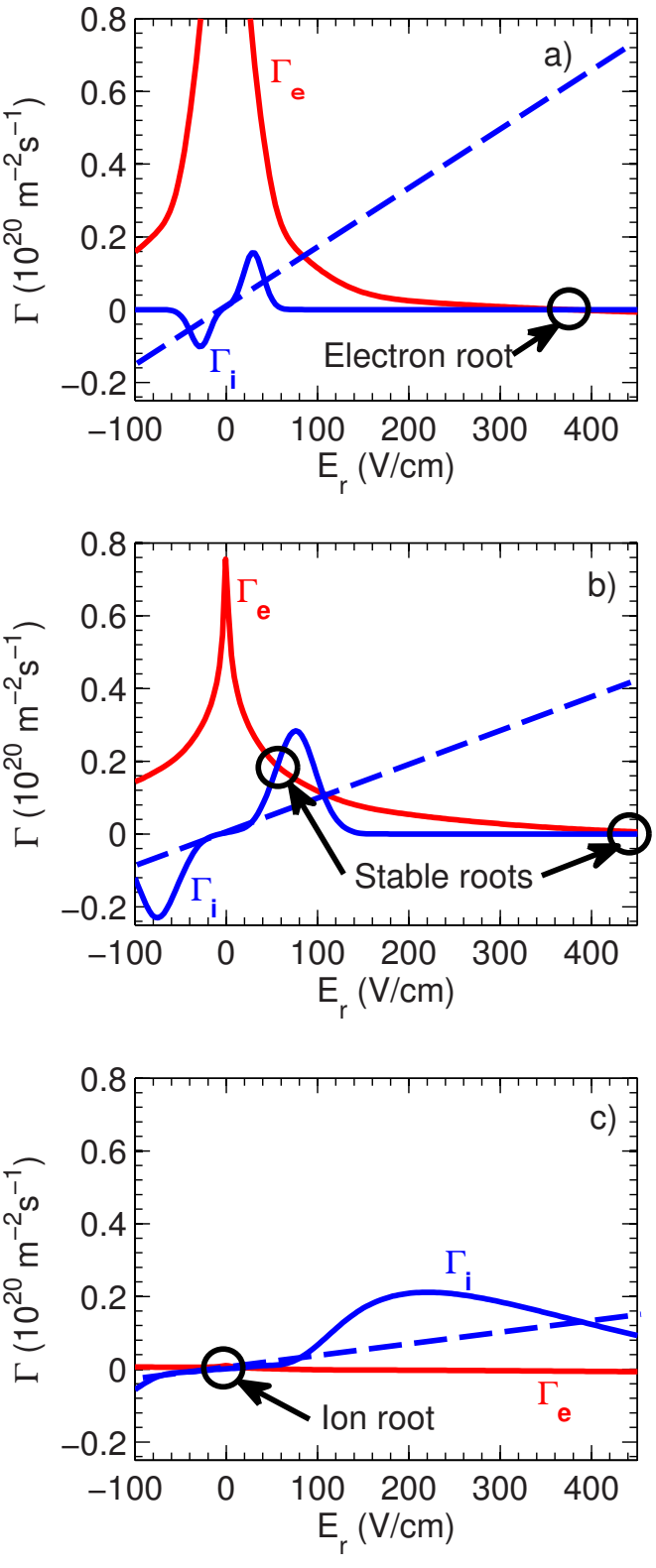

FIG. 4. (Color online) Neoclassical particle fluxes vs E_r for three different radii. (a) r/a=0.1, T_e=2 keV, T_i=70 eV; (b) r/a=0.3, T_e=750 eV, T_i=60 eV; (c) r/a=0.5, T_e=300 eV, T_i=55 eV. Ion particle flux ignoring the effect of the resonance is shown for reference (dashed line).

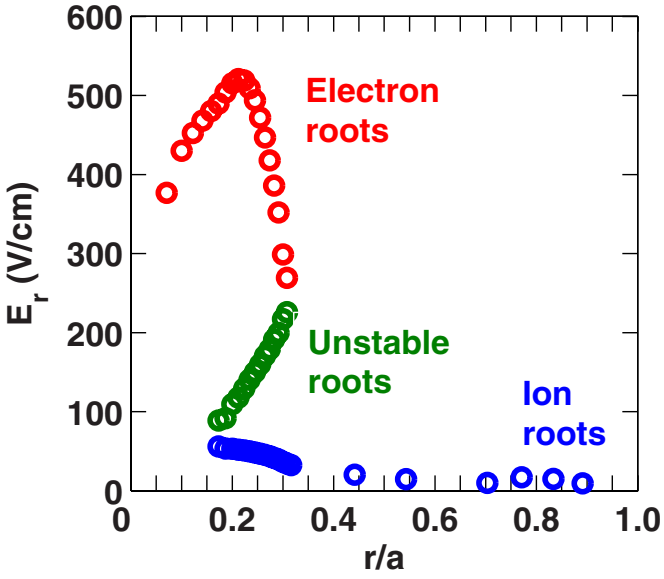

FIG. 5. (Color online) Neoclassically predicted radial electric field profile for the profiles shown in Fig. 2.

tions exist near E_r=0. Note that the ion root solutions near the plasma edge are small and typically positive (opposed to negative in the case shown in Fig. 1) because the ions are not collisionless enough to be in the "1/ν" regime, therefore the flux at E_r=0 is small. This scenario of achieving core electron root solutions due to the large ratio of T_e/T_i and a reduction in Γ_i from the resonance is different than most stellarators that observe CERCs, with the exception of ECRH heated W7-AS plasmas.

The critical feature of the E_r profile shown in Fig. 5 is that with only electron root solutions near the core, and only ion root solutions near the edge, a transition must occur in the multiple root region, with significant radial shear. The location of this "shear layer" can be calculated by including the effect of the perpendicular viscosity.[44,45,41] A finite perpendicular viscosity modifies the standard ambipolarity constraint and results in a diffusion equation for the radial electric field,[41,44–46,10]

$$\frac{\partial E_r}{\partial t} - \frac{\partial}{\partial V}\left[\langle \nabla V\rangle D_E\left(\frac{\partial E_r}{\partial r} - \frac{E_r}{r}\right)\right] = \frac{e}{\varepsilon_\perp}(\Gamma_e - \Gamma_i), \qquad (6)$$

where V is the volume enclosed by the surface labeled with r and $\varepsilon_\perp \equiv M_{eff}\varepsilon_0(1+c^2/V_A^2)$ with V_A the Alfven velocity and c the speed of light in vacuum. The enhancement factor $M_{eff} \cong 1+2q^2$,[47] where for HSX the effective rotational transform $\iota = 1/q \approx 3$, has been taken to be unity for this work. The flux surface average operator is given by $\langle \cdots \rangle \equiv \int\int d\theta d\phi \sqrt{g}(\cdots)/\int\int d\theta d\phi \sqrt{g}$, where $\sqrt{g}$ is the Jacobian for the coordinates (r, θ, ϕ) with ϕ and θ representing toroidal and poloidal angles, respectively. The radial electric field "diffusion coefficient" D_E is related to the perpendicular viscosity[44] and is not known for general configurations. Figure 6(a) shows the solutions to Eq. (6) for several values of D_E. The coefficient D_E can, in principle, be calculated from neoclassical theory[48,49] or estimated from the ion diffusion

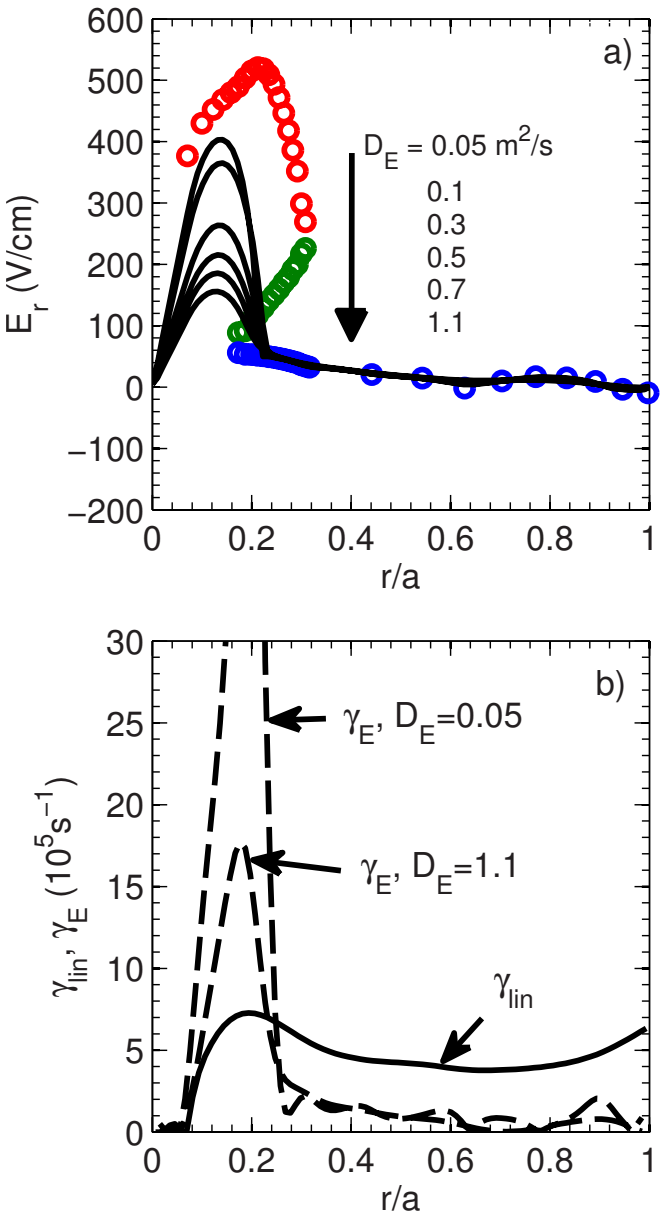

FIG. 6. (Color online) (a) Ambipolar radial electric field profile and solutions to Eq. (6) for several values of D_E. (b) Growth rates calculated from experimental profiles and shearing rates corresponding to two extreme values of D_E.

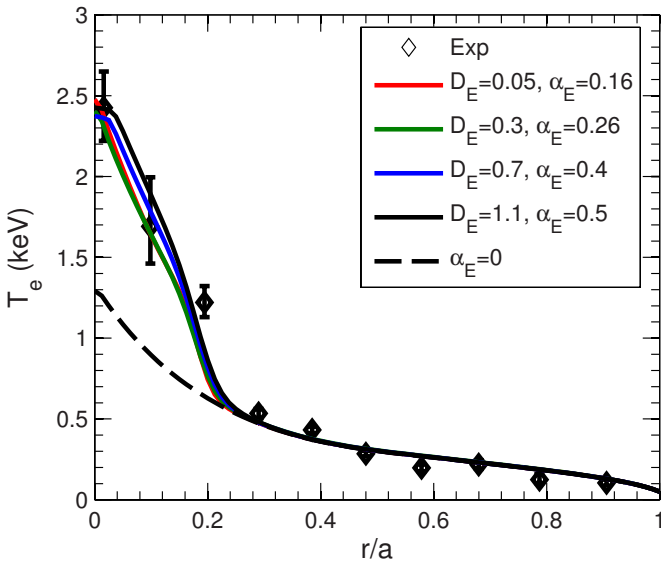

FIG. 7. (Color online) Simulated and measured electron temperature profiles. Simulated profiles are shown with and without effect of E×B shear suppression, for a range of α_E and D_E.

IV. PREDICTIVE TRANSPORT SIMULATIONS

Turbulent transport has been modeled in the QHS configuration of HSX using the axisymmetric quasilinear Weiland model.[50–52] Use of the Weiland model is justified in QHS because, like in a tokamak, the transport is dominated by a single class of trapped particles. Further, with local geometry considerations (specifically, replacing the toroidal curvature with the helical curvature and using the appropriate trapped particle fraction) good agreement is found with growth rates calculated from the three-dimensional gyrokinetic code GS2 (Refs. 53 and 54) for experimentally relevant gradients.[10] The applied model has also successfully predicted zero-dimensional transport quantities such as the stored energy and energy confinement times within 10% of experimental values.[10] For a detailed description of turbulent transport modeling for HSX, see Refs. 10 and 55.

Predictive transport simulations were performed to evolve the electron temperature using the one-dimensional transport equation,

$$\frac{3}{2}n_e\frac{\partial T_e}{\partial t} - \frac{\partial}{\partial V}\langle\nabla V\rangle Q_e = P_{\mathrm{ECRH}}(r), \tag{7}$$

and the radial electric field using Eq. (6). In Eq. (7) the heat flux Q_e is the sum of the neoclassical and turbulent contributions, and the ECRH power deposition profile is calculated using a ray-tracing code,[56,57] normalized to give the total absorbed power measured from the time response of the diamagnetic loop at ECRH turnoff. Other power sinks and sources have been neglected for these simulations.

The measured and simulated electron temperature profiles for a 100 kW QHS plasma *neglecting* the effect of sheared flow are shown in Fig. 7 (symbols and dashed line, respectively). The temperatures have been greatly underestimated inside of $r/a \approx 0.3$, the radius where the T_e profile becomes peaked. In this region the neoclassical transport is small due to the large E_r, therefore it is the turbulent trans-

coefficient[41] (as the neoclassical perpendicular viscosity should be driven by ion drifts coupling neighboring flux surfaces). In the latter case, using $D_E=D_{11i}(E_r)$ results in an extremely sharp transition because the ion diffusion coefficient is very small for the QHS parameters discussed here (<0.1 m^2/s). On the other hand, assuming a turbulence-driven D_E (on the order of χ_e, for example) would give a value of 0.3–0.7 m^2/s in the core region. For any value in this range, the solution to Eq. (6) results in a region of strong radial E_r shear at $r/a \approx 0.25$, which is near the location where the T_e profile becomes strongly peaked (compare Fig. 2). This strong E_r shear has a significant impact on the turbulent transport when performing predictive transport simulations.

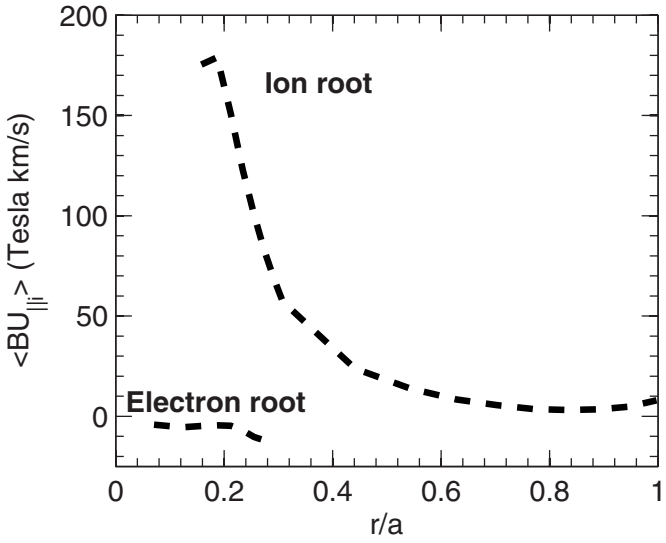

FIG. 8. Neoclassically predicted ion parallel flow profile. Upper curve corresponds to ion root solutions and lower curve to electron root (see Fig. 5).

port that limits the simulated T_e. The calculated growth rates from the Weiland model and GS2 remain in good agreement at $r/a \approx 0.25$, suggesting that a mechanism of turbulent transport suppression is required. Given the strong E_r shear in this region, turbulence quenching via $\mathbf{E}\times\mathbf{B}$ flow shear is a viable mechanism.

The suppression of turbulent transport is included through a linear "quench rule"[58] where the turbulent diffusivity is scaled by $\max(1-\alpha_E\gamma_E/\gamma_{\max},0)$. The shearing rate γ_E is given by $(r/q)\,\partial(qv_{E\times B}/r)/\partial r$ and $\gamma_{\max}$ is the maximum linear growth rate. Figure 6(b) shows the model linear growth rate, calculated from the experimental profiles, and γ_E for two extreme values of D_E, 0.05 and 1.1 m^2/s. For each D_E, α_E was chosen to reproduce the peak experimental temperature, as shown in Fig. 7. The values of D_E and α_E required to reproduce the experimental profiles are clearly coupled, for example, a smaller D_E requires a smaller α_E. Nonlinear tokamak simulations have found that a value of $\alpha_E \approx 0.5$ is able to reproduce the suppression of trapped electron mode-dominant turbulence,[58] which is expected to dominate QHS transport.[10] For stellarators, the scale factor is not known. A tokamaklike value of $\alpha_E \approx 0.5$ only requires a modest amount of shear, corresponding to $D_E = 1.1$ m^2/s, see Fig. 6(a). For any value of D_E in the range shown, the shearing rate is much larger than the linear growth rate for $0.1 < r/a < 0.3$, and quenching would be expected in this region. Similar values of D_E have been shown to give good agreement with measured E_r profiles in W7-AS.[46,59]

V. EFFECT OF MOMENTUM CONSERVATION AND LARGE E_r ON TRANSPORT

The momentum-conserving neoclassical calculations described in Sec. II result in significant parallel ion flows $\langle BU_{\|i}\rangle$, as shown in Fig. 8 for the profiles given in Fig. 2. A region of two solutions exists near the core, corresponding to the ion and electron root ambipolar E_r solutions, compare to Fig. 5. Measurements from the ChERS diagnostic give parallel flows on the order of 10–20 km/s across the plasma radius.[60] At present, the lack of spatial resolution in the core[61] precludes a direct comparison to ChERS data, but improvements are in progress with results to be presented in the future. Inside of $r/a \approx 0.4$ the flows corresponding to the neoclassical ion root predictions become very large, reaching speeds on the order or larger than the ion thermal velocity v_{Ti} ($\sim$140 km/s for 100 eV protons). These large flows violate the assumption of $U_{\|i} \ll v_{Ti}$ made in the neoclassical analysis, in which stationary Maxwellians are used.[22] In the QHS configuration of HSX, the flow should be dominant in the $(n,m)=(4,1)$ helical direction. Recent ChERS measurements indicate that the flow in the symmetry direction is a factor of $\sim$10 larger than the flow in the ∇B direction on a flux surface.[61]

The effect of momentum conservation on the neoclassical flux in QHS is shown in Fig. 9(a). For $E_r \leq E_r^{\text{res}}$ the ion flux accounting for momentum conservation is $\sim 25\%-30\%$ smaller than without momentum conservation. When $E_r > E_r^{\text{res}}$ the effect is minimal because the ion flux has been reduced to a very small level by the resonance. The electron flux, on the other hand, is nearly identical in both cases. The change in the ion flux modifies the ambipolar ion root solution, while the electron root is largely unchanged, as shown in Fig. 10. Due to these effects, the changes in the ion particle flux and ion root E_r are rather small for current HSX experimental parameters (small T_i, $T_e \gg T_i$). At higher T_i, ion root solutions are likely to exist across the plasma radius due to the reduced ratio of T_e/T_i. In this case the ion root would act to reduce the ion transport from the $E_r=0$ level, and E_r must be known precisely to calculate the steady-state transport quantities.

HSX also has the option of running in a spoiled symmetry configuration, where a set of planar coils are energized to produce $m=0$ "mirror" terms in the magnetic spectrum. In this configuration, the flow damping is larger on a flux surface, and the effect of momentum conservation should be reduced as compared to QHS. Figure 9(b) shows the neoclassical fluxes versus E_r in the spoiled symmetry configuration for the same temperature and density profiles used in Fig. 9(a). The ion fluxes *without* momentum conservation are almost identical in Figs. 9(a) and 9(b), indicating that the increased ripple transport in the spoiled symmetry configuration does not affect ions at this temperature ($T_i \leq 100$ eV). The electron flux, on the other hand, is greatly increased in the spoiled symmetry configuration because the electrons are in the LMPF regime. The effect of including momentum conservation on the ion flux is much larger in QHS than with the symmetry spoiled, as expected using a simple flow damping argument. Note that the larger electron flux in the spoiled symmetry configuration acts to increase or even remove the ambipolar ion root solution as compared to QHS (the latter case is shown in Fig. 9). It also results in a broader region where only electron root solutions exist in the core, which may act to move the location of the strong E_r shear outward. On the other hand, the electron confinement at a given set of parameters ($T_e, \nabla T_e, E_r, \ldots$) is degraded.

As mentioned in Sec. II, the large ($E_r \gg E_r^{\text{res}}$) radial electric fields predicted in QHS can present problems in the neo-

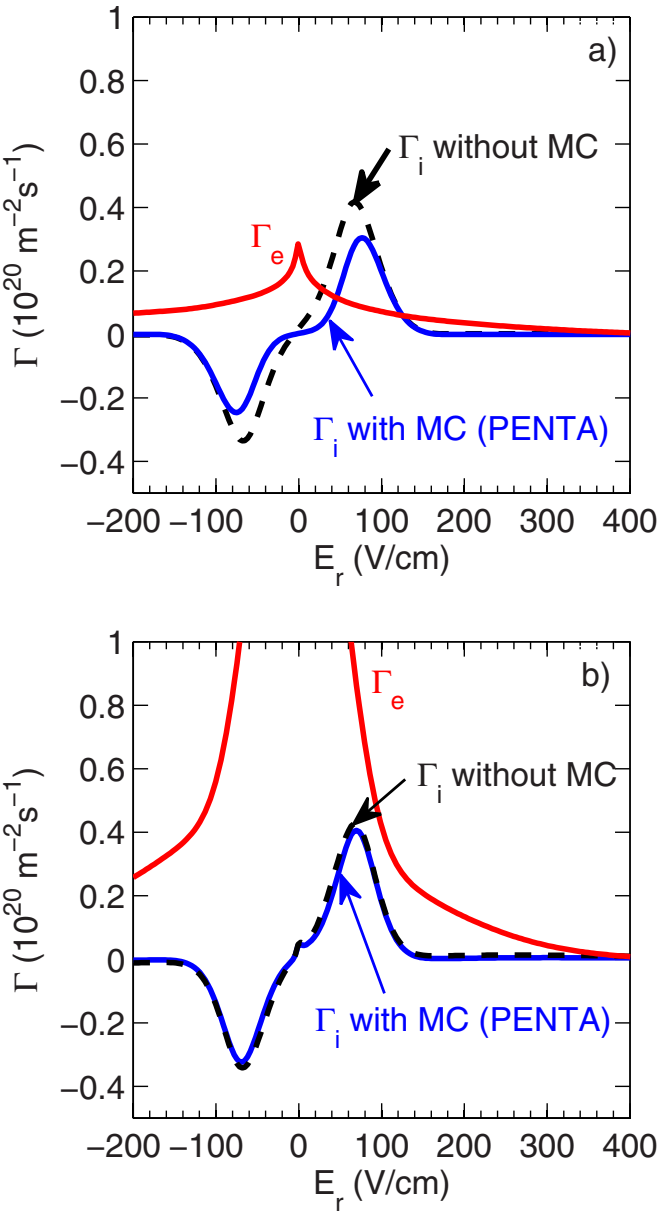

FIG. 9. (Color online) Neoclassical particle fluxes vs E_r with and without the effect of momentum conservation (MC). (a) In the QHS configuration and (b) in the spoiled symmetry configuration for the same input profiles. The effect of MC on the electron flux is minimal.

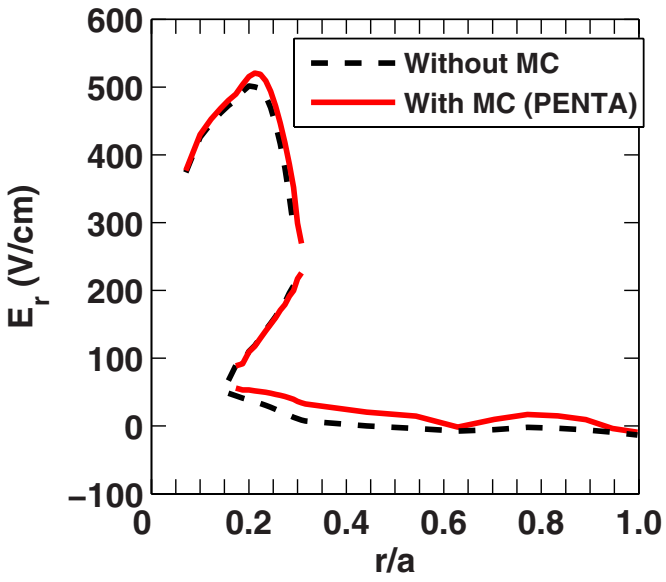

FIG. 10. (Color online) Predicted radial electric field profiles with and without momentum conservation (MC).

classical transport analysis. The *local* and *monoenergetic* approximations made when ordering the DKE in many neoclassical transport algorithms, including DKES, reduce a five-dimensional problem to three dimensions. This allows for relatively fast and efficient computation of the full neoclassical transport matrix of radial transport, bootstrap current, and parallel conductivity coefficients. Particles near the resonance, however, experience large drifts with unusual orbits[62] and significant deviations in energy,[63] not captured in DKES due to the assumption of incompressible $\mathbf{E}\times\mathbf{B}$ flow. The change in the energy has been observed numerically to "smooth" the resonant behavior seen in the DKES data, but not significantly change the results for $E_r/E_r^{\mathrm{res}}<0.5-0.7$. The effect of the change in energy was also shown to be small for E_r much larger than the resonance (on the order of ~2x larger), that is, the strong reduction in D_{11} for $E_r \gg E_r^{\mathrm{res}}$ still exists.[63] This agreement is not valid when multiple resonances (due to complex $|B|$ spectrum) exist, but may be acceptable for the single dominant resonance observed in QHS. A broadening, or smoothing, of the resonance would act to modify the E_r roots at the sides of the three root region seen in Fig. 5. As the strong E_r shear is caused by the radial proximity of the regions of *only* ion or electron root solutions, and the electron root region in the core occurs for $E_r \gg E_r^{\mathrm{res}}$ one may expect the overall effect to be unimportant to the results presented here. In addition, ECRH plasmas at W7-AS included the effect of the resonance to explain very large electron root solutions in the core, and good agreement was seen between measured and predicted E_r profiles.[13]

The large E_r can also affect the momentum-conserving treatment described in Sec. II. In the moment method momentum correction techniques discussed here, see Refs. 29 and 33, as well as in traditional neoclassical transport theory,[64] the radial transport of parallel momentum is neglected in the parallel momentum balance. This approximation, however, is only valid for $E_r \ll E_r^{\mathrm{res}}$,[33] which is more restrictive than the limit imposed by the assumption of monoenergtic particles. This effect may be important when estimating neoclassical quantities very near the core of QHS plasmas.

VI. SUMMARY AND CONCLUSIONS

The effect of a neoclassically determined radial electric field profile on electron heat transport in HSX has been described. The large ratio of T_e/T_i, coupled with the reduction in ion transport due to the poloidal resonance, leads to a radial electric field profile with only electron root solutions in the core and only ion root solutions across most of the plasma radius. In an intermediate region of multiple roots a transition occurs. The transition can be estimated using a

diffusion equation for E_r, resulting in significant radial shear in the same region where the measured T_e profile is centrally peaked.

The large radial electric field in the core acts to reduce the neoclassical transport, while the strong radial shear quenches the turbulent transport. Turbulent transport is modeled using the Weiland model, which has been shown to agree well with growth rates from GS2 for experimentally relevant gradients after appropriate geometry corrections have been made. Predictive transport simulations overestimate the core transport unless the effect of shear suppression is included using a linear quench rule. The central peaking of the T_e profile can be reproduced for a range of quenching scale factors α_E and radial electric field diffusion coefficients D_E, which are consistent with values used in other stellarators and in tokamak simulations.

Neoclassical transport calculations are performed using the PENTA code, which is based on a moment method that conserves momentum by accounting for the parallel flows. The effect of momentum conservation is important in (quasi)symmetric systems, which have reduced flow damping in the direction of symmetry. PENTA predicts significant parallel flows across the plasma radius. In the core very large flows violate the assumption of $U_{\|i} \ll v_{Ti}$; ChERS measurements (to be presented elsewhere) may shed light on the consequences of this assumption. The momentum correction technique results in modified ion fluxes, as compared to direct energy convolution of the DKES coefficients. The impact of the reduced ion flux given by PENTA is small for current QHS experimental parameters. When the symmetry is spoiled, the effect of the momentum correction is reduced for the same plasma profiles. On the other hand, the increased electron flux in the symmetry breaking configuration results in a larger region where only electron root solutions exist in the core. This observation raises the question of whether there is an optimal amount of symmetry breaking that allows the location of the E_r shear and T_e peaking to occur at a large radius (and therefore improve confinement over a larger volume), and whether this effect outweighs the increased ripple transport.

ACKNOWLEDGMENTS

The authors acknowledge helpful discussions with H. Sugama, S. Nishimura, and C. D. Beidler. This work is supported by DOE Grant No. DE-FG02-93ER54222.

[1] F. S. B. Anderson, D. T. Anderson, A. Almagri, P. G. Matthews, J. N. Talmadge, and J. L. Shohet, Fusion Technol. **27**, 273 (1995).
[2] A. H. Boozer, Phys. Fluids **26**, 496 (1983).
[3] H. E. Mynick, Phys. Plasmas **13**, 058102 (2006).
[4] S. P. Gerhardt, J. N. Talmadge, J. M. Canik, and D. T. Anderson, Phys. Rev. Lett. **94**, 015002 (2005).
[5] D. A. Spong, Phys. Plasmas **12**, 056114 (2005).
[6] P. Helander and A. N. Simakov, Phys. Rev. Lett. **101**, 145003 (2008).
[7] J. M. Canik, D. T. Anderson, F. S. B. Anderson, K. M. Likin, J. N. Talmadge, and K. Zhai, Phys. Rev. Lett. **98**, 085002 (2007).
[8] J. N. Talmadge, F. S. B. Anderson, D. T. Anderson, C. Deng, W. Guttenfelder, K. M. Likin, J. Lore, J. C. Schmitt, and K. Zhai, J. Plasma Fusion Res. **3**, S1002 (2008).
[9] C. B. Deng, D. L. Brower, B. N. Breizman, D. A. Spong, A. F. Almagri, D. T. Anderson, F. S. B. Anderson, W. X. Ding, W. Guttenfelder, K. M. Likin, and J. N. Talmadge, Phys. Rev. Lett. **103**, 025003 (2009).
[10] W. Guttenfelder, J. Lore, D. T. Anderson, F. S. B. Anderson, J. M. Canik, W. Dorland, K. M. Likin, and J. N. Talmadge, Phys. Rev. Lett. **101**, 215002 (2008).
[11] W. Guttenfelder, D. T. Anderson, F. S. B. Anderson, J. M. Canik, K. M. Likin, and J. N. Talmadge, Phys. Plasmas **16**, 082508 (2009).
[12] A. Fujisawa, H. Iguchi, H. Sanuki, K. Itoh, S.-I. Itoh, S. Okamura, K. Matsuoka, and Y. Hamada, Plasma Phys. Controlled Fusion **40**, 627 (1998).
[13] J. Baldzuhn, M. Kick, H. Maaßberg, and the W7-AS Team, Plasma Phys. Controlled Fusion **40**, 967 (1998).
[14] Y. Takeiri, T. Shimozuma, S. Kubo, S. Morita, M. Osakabe, O. Kaneko, K. Tsumori, Y. Oka, K. Ikeda, K. Nagaoka, N. Ohyabu, K. Ida, M. Yokoyama, J. Miyazawa, M. Goto, K. Narihara, I. Yamada, H. Idei, Y. Yoshimura, N. Ashikawa, M. Emoto, H. Funaba, S. Inagaki, M. Isobe, K. Kawahata, K. Khlopenkov, T. Kobuchi, A. Komori, A. Kostrioukov, R. Kumazawa, Y. Liang, S. Masuzaki, T. Minami, T. Morisaki, S. Murakami, S. Muto, T. Mutoh, Y. Nagayama, Y. Nakamura, H. Nakanishi, Y. Narushima, K. Nishimura, N. Noda, S. Ohdachi, T. Ozaki, B. J. Peterson, A. Sagara, K. Saito, S. Sakakibara, R. Sakamoto, M. Sasao, K. Sato, M. Sato, T. Seki, M. Shoji, H. Suzuki, N. Tamura, K. Tanaka, K. Toi, T. Tokuzawa, K. Y. Watanabe, T. Watari, Y. Xu, H. Yamada, M. Yoshinuma, K. Itoh, K. Ohkubo, T. Satow, S. Sudo, T. Uda, K. Yamazaki, Y. Hamada, K. Matsuoka, O. Motojima, M. Fujiwara, T. Notake, N. Takeuchi, Y. Torii, S. Yamamoto, T. Yamamoto, T. Akiyama, P. Goncharov, T. Saida, H. Kawazome, and H. Nozato, Phys. Plasmas **10**, 1788 (2003).
[15] F. Castejón, V. Tribaldos, I. García-Cortés, E. de la Luna, J. Herranz, and I. Pastor, T. Estrada, and the TJ-II Team, Nucl. Fusion **42**, 271 (2002).
[16] M. Yokoyama, H. Maaßberg, C. D. Beidler, V. Tribaldos, K. Ida, F. Castejón, T. Estrada, A. Fujisawa, T. Minami, T. Shimozuma, Y. Takeiri, J. Herranz, S. Murakami, and H. Yamada Fusion Sci. Technol. **50**, 327 (2006).
[17] M. Yokoyama, H. Maaßberg, C. D. Beidler, V. Tribaldos, K. Ida, T. Estrada, F. Castejón, A. Fujisawa, T. Minami, T. Shimozuma, Y. Takeiri, A. Dinklage, S. Murakami, and H. Yamada, Nucl. Fusion **47**, 1213 (2007).
[18] U. Stroth, K. Itoh, S.-I. Itoh, H. Hartfuss, H. Laqua, the ECRH Team, and the W7-AS Team, Phys. Rev. Lett. **86**, 5910 (2001).
[19] J. García, K. Yamazaki, J. Dies, and J. Izquierdo, Phys. Rev. Lett. **96**, 105007 (2006).
[20] M. Hirsch, J. Baldzuhn, C. Beidler, R. Brakel, R. Burhenn, A. Dinklage, H. Ehmler, M. Endler, V. Erckmann, Y. Feng, J. Geiger, L. Giannone, G. Greiger, P. Grigull, H.-J. Hartfuß, D. Hartmann, R. Jaenicke, R. König, H. P. Laqua, H. Maaßberg, K. McCormick, F. Sardei, E. Speth, U. Stroth, F. Wagner, A. Weller, A. Werner, H. Wobig, and S. Zoletnik for the W7-AS Team, Plasma Phys. Controlled Fusion **50**, 053001 (2008).
[21] H. Maaßberg, C.D. Beidler, U. Gasparino, M. Romé, the W7-AS Team, K. S. Dyabilin, N. B. Marushchenko, and S. Murakami, Phys. Plasmas **7**, 295 (2000).
[22] H. Sugama and S. Nishimura, Phys. Plasmas **9**, 4637 (2002).
[23] See, for example, K. C. Shaing, Phys. Rev. Lett. **76**, 4364 (1996).
[24] K. C. Shaing and J. D. Callen, Phys. Fluids **26**, 3315 (1983).
[25] M. Coronado and J. N. Talmadge, Phys. Fluids B **5**, 1200 (1993).
[26] S. P. Hirshman, K. C. Shaing, W. I. van Rij, C. O. Beasley, Jr., and E. C. Crume, Jr., Phys. Fluids **29**, 2951 (1986).
[27] W. I. van Rij and S. P. Hirshman, Phys. Fluids B **1**, 563 (1989).
[28] S. P. Hirshman and D. J. Sigmar, Nucl. Fusion **21**, 1079 (1981).
[29] H. Sugama and S. Nishimura, Phys. Plasmas **15**, 042502 (2008).
[30] H. Sugama and W. Horton, Phys. Plasmas **3**, 304 (1996).
[31] P. Helander and D. J. Sigmar, *Collisional Transport in Magnetized Plasmas* (Cambridge University Press, Cambridge, 2002), p. 278.
[32] M. Taguchi, Phys. Fluids B **4**, 3638 (1992).
[33] H. Maaßberg, C. D. Beidler, and Y. Turkin, Phys. Plasmas **16**, 072504 (2009).
[34] L. Spitzer and R. Härm, Phys. Rev. **89**, 977 (1953).
[35] A. Matsuyama, M. Yu. Isaev, K. Y. Watanabe, K. Hanatani, N. Nakajima, W. A. Cooper, and T. M. Tran, Phys. Plasmas **16**, 052501 (2009).
[36] K. C. Shaing, Phys. Fluids **29**, 2231 (1986).
[37] H. E. Mynick and W. N. G. Hitchon, Nucl. Fusion **23**, 1053 (1983).
[38] M. Romé, C. D. Beidler, H. Maaßberg, N. B. Marushchenko, Yu. A. Turkin, and the W7-AS Team, Plasma Phys. Contr. Fusion **48**, 353 (2006).
[39] A. R. Briesemeister, K. Zhai, and F. S. B. Anderson, Bull. Am. Phys. Soc. **52**(16), 253 (2007).
[40] H. P. Summers, 2004, *The ADAS User Manual*, version 2.6, University of Strathclyde, 107 Rottenrow, Glasgow G4 0NG, United Kingdom, http://www.adas.ac.uk.

[41]H. Maaßberg, R. Burhenn, U. Gasparino, G. Kühner, H. Ringler, and K. S. Dyabilin, Phys. Fluids B **5**, 3627 (1993).
[42]M. Yokoyama, M. Wakatani, and K. C. Shaing, Nucl. Fusion **35**, 153 (1995).
[43]A. A. Galeev and R. Z. Sagdeev, Sov. Phys. JETP **26**, 233 (1968).
[44]D. E. Hastings, W. A. Houlberg, and K. C. Shaing, Nucl. Fusion **25**, 445 (1985).
[45]K. C. Shaing, Phys. Fluids **27**, 1567 (1984).
[46]H. Ehmler, Y. Turkin, C. D. Beidler, H. Maaßberg, A. Dinklage, T. Klinger, and the W7-AS Team, Nucl. Fusion **43**, L11 (2003).
[47]K. Itoh and S.-I. Itoh, Plasma Phys. Controlled Fusion **38**, 1 (1996).
[48]D. E. Hastings, Phys. Fluids **28**, 334 (1985).
[49]D. E. Hastings, Phys. Fluids **27**, 458 (1984).
[50]H. Nordman, J. Weiland, and A. Jarmén, Nucl. Fusion **30**, 983 (1989).
[51]G. Bateman, A. H. Kritz, J. E. Kinsey, A. J. Redd, and J. Weiland, Phys. Plasmas **5**, 1793 (1998).
[52]J. Weiland, *Collective Modes in Inhomogeneous Plasmas* (IOP, Bristol, 2000).
[53]M. Kotschenreuther, G. Rewoldt, and W. M. Tang, Comput. Phys. Commun. **88**, 128 (1995).
[54]W. Dorland, F. Jenko, M. Kotschenreuther, and B. N. Rogers, Phys. Rev. Lett. **85**, 5579 (2000).
[55]W. A. Guttenfelder, Ph.D. thesis, University of Wisconsin-Madison, 2007.
[56]R. C. Goldfinger, D. K. Lee, K. M. Likin, and B. D. Ochirov, Nucl. Fusion **31**, 2305 (1991).
[57]K. M. Likin and B. D. Ochirov, Sov. J. Plasma Phys. **18**, 42 (1992).
[58]J. E. Kinsey, R. E. Waltz, and J. Candy, Phys. Plasmas **12**, 062302 (2005).
[59]Yu. Turkin, H. Maaßberg, C. D. Beidler, J. Geiger, and N. B. Marushchenko, Fusion Sci. Technol. **50**, 387 (2006).
[60]A. R. Briesemeister, K. Zhai, D. T. Anderson, J. Lore, and J. N. Talmadge, Bull. Am. Phys. Soc. **54**(15), 287 (2009).
[61]A. Briesemeister, K. Zhai, D. T. Anderson, F. S. B Anderson, J. Lore and J. N. Talmadge, "Flow velocity measurements using ChERS in the HSX Stellarator," Contrib. Plasma Phys. (to be published).
[62]B. D. de Gevigney, T. Sunn Pedersen, and A. H. Boozer, Bull. Am. Phys. Soc. **53**(14), 62 (2008).
[63]C. D. Beidler, M. Yu. Isaev, S. V. Kasilov, W. Kernbichler, H. Maaßberg, S. Murakami, V. V. Nemov, D. A. Spong, and V. Tribaldos, *Proceedings of the 17th International Toki Conference and 16th International Stellarator/Heliotron Workshop*, Toki, 2007 (NIFS-PROC Series Research Report, Toki, 2007), p. 623.
[64]See, for example, F. L. Hinton and R. D. Hazeltine, Rev. Mod. Phys. **48**, 239 (1976).